JOURNAL OF CATALYSIS 100, 437–445 (1986)

Electron Microdiffraction Study of Bimetallic Ru–Au/MgO Catalysts

A. G. SHASTRI AND J. SCHWANK

Department of Chemical Engineering, The University of Michigan, Ann Arbor, Michigan 48109-2136

Received December 23, 1985

A microdiffraction study of bimetallic Ru–Au/MgO catalysts is carried out in order to discriminate between the random adsorption versus atomic ordering model proposed for the structure of bimetallic clusters. The microdiffraction patterns from small metal clusters could be ascribed to either Au or Ru indicating an absence of structural modification of individual metal components in bimetallic clusters. Local variations in the MgO planes exposed are seen within areas of 1 μm in diameter which are free of metal particles. Large Au particles (>10 nm) are randomly aligned on MgO whereas small Au particles are aligned such that the [110] zone axis of Au is parallel to the [111] zone axis of MgO. Small Ru particles are aligned so that in most cases the [0001] zone axis of Ru is parallel to the [111] zone axis of MgO. The random adsorption model, where one metal component is chemisorbed on top of the other, is consistent with the experimental observations by EDS and microdiffraction.

INTRODUCTION

Bimetallic catalyst systems comprised of active Group VIII metal and inactive Group Ib metal have been of significant research interest, since they allow one to study the role of geometric and electronic effects in catalysis (*1*). Supported Ru–Au catalysts (*2–12*) have been investigated by a variety of techniques to elucidate the correlation between the microstructure and activity of the catalysts. These catalysts allow one to address the question of bimetallic cluster formation for small particles (<5 nm) as the metals Ru and Au are immiscible in the bulk. For SiO_2- and MgO-supported Ru–Au catalysts, recent work including catalytic activity measurements (*8*), analytical electron microscopy (*7, 21*), and chemisorption/surface titration procedures (*10–12*) has clearly shown the presence of bimetallic clusters. Energy dispersive X-ray spectroscopy (EDS) has proved the presence of both metals in small (<5 nm) particles (*7, 12*). Sinfelt *et al.* (*1*) have advanced the hypothesis that the bimetallic clusters in these bulk immiscible systems are comprised of one metal component randomly adsorbed on top of the other. Other investigators have proposed that there should be some ordering in the spatial atomic distribution in small bimetallic clusters which can be described within the regular solution theory (*13*). It is not possible to distinguish between Sinfelt's random adsorption model (*1*) versus the atomic ordering model (*13*) for small bimetallic clusters in bulk immiscible systems by EDS or catalytic activity data alone. Structural information on these small bimetallic particles is needed to decide between the adsorption versus atomic ordering model. In particular, it is of fundamental interest to understand whether the bulk immiscibility is violated for such small bimetallic clusters. Electron microdiffraction seems to be a promising technique to provide such information with good spatial resolution (*14–21*). With the use of field emission guns in scanning transmission electron microscopes, it is possible to generate a probe as small as 0.5 nm in size, allowing one to gain structural insight from very small regions (*14*). Moreover, microdiffraction gives information about the alignment of small metal particles on oxide substrates.

0021-9517/86 $3.00

Previous work has clearly shown a significant influence of small metal particles (Au) on the properties of insulating (MgO) or semiconducting (TiO_2) oxide materials (*28*). It has also been reported that heating of evaporated Au deposits on MgO under moderate vacuum results in a solid state reaction causing an etching of the MgO surface (*29*). In spite of the power of microdiffraction as a structural probe, relatively few papers have been published on the application of the technique to supported catalysts, the main reason being that a careful analysis of a large number of microdiffraction patterns and comparison with computer-simulated diffraction patterns based on the multislice formulation of dynamical theory (*31*) becomes necessary for data interpretation. A microdiffraction study of Pt and Pd particles on alumina did not show any preferred metal particle/support orientation (*32*). However, an epitaxial relationship was observed between Cu and ZnO, such that Cu [111] and ZnO [0002] axes were parallel (*33*).

Our objective for this study was to apply microdiffraction to MgO-supported bimetallic Ru–Au catalysts in order to discriminate between the two models for the structure of bimetallic particles mentioned earlier. Previous work on these Ru–Au/MgO catalysts has shown the presence of bimetallic clusters in a metal particle size range of less than 5 nm (*12*). The information derived from microdiffraction patterns of different specimen areas is used to gain insight into the relative alignment of metal particles with the oxide support and the structure of oxide in the vicinity of metal particles.

EXPERIMENTAL

The catalysts were prepared by coimpregnation of MgO (Carlo Erba, reagent grade) with aqueous solutions of $RuCl_3 \cdot H_2O$ (Rudi-Pont reagent grade) and $HAuCl_4 \cdot 3H_2O$ (Carlo Erba RPE). After drying the samples at 388 K for 4 h in air, the samples were stirred in a 0.5 *M* NaOH solution of hydrazine to facilitate reduction. This was followed by another drying step at 388 K. Each catalyst was assigned a code, containing the letter R for Ru, M for MgO, H for hydrazine reduction, and a three-digit number representing the atomic percentage of Ru out of the total metal content in the catalyst. Aliquots of these hydrazine reduced samples were subsequently pretreated in H_2 at 673 K for 24 h before TEM and microdiffraction experiments. Table 1 summarizes some of the pertinent characterization data obtained from previous work (*12*).

For electron microscopy specimen preparation, a very small amount of the sample was stirred in reagent grade isopropanol. A drop of the suspension was placed on a holey carbon film covered copper grid. Specimen areas in the holes of the carbon film were selected for TEM imaging and microdiffraction. A JEOL-100 CX microscope equipped with a side-entry goniometer stage, ASID-4D scanning attachment, lithium drifted solid-state X-ray detector, and a multichannel analyzer/ND6620 computer system was used. The sample height was kept at the eucentric position for all experiments. Numerous TEM pictures of each sample were taken to derive representative particle size distributions. For microdiffraction, a suitable specimen area was first identified and focused in the STEM mode of the electron microscope. A condenser aperture of 20 μm was then inserted and centered in the TEM mode. The microscope was again switched over to the STEM mode and the selected specimen area was carefully refocused. An electron probe of 10 nm was held stationary on the specimen area of interest and microdiffraction patterns were examined by lowering the TEM screen. Diffraction patterns were photographed with suitable exposure times. The camera length was determined for various values of lens currents and specimen position by obtaining microdiffraction patterns from a polycrystalline Au film standard. No specimen tilting was done in any

TABLE 1

Summary of Characterization Data

Sample code	Metal loading (wt%)		Average particle size by TEM[a] (nm)			Allocation of metal in a given particle size range (nm)		
						<5	5–10	>10
	Ru	Au	d_n	d_s	d_v			
RMH093	3.28	0.468	3.7	5.2	6.5	Ru Ru + trace Au	Ru	Au
RMH014	0.26	3.109	8.9	13.1	19.9	Ru + trace Au Au + trace Ru	Au	Au

[a] d_n = number average = $\Sigma n_i d_i / \Sigma n_i$, d_s = surface average = $\Sigma n_i d_i^3 / \Sigma n_i d_i^2$, d_v = volume average = $\Sigma n_i d_i^4 / \Sigma n_i d_i^3$, where n_i is the number of particles of size d_i.

of the experiments. Many different regions of the specimen were examined in order to get a representative picture.

RESULTS AND DISCUSSION

Figure 1 shows the representative TEM pictures for each sample. Metal particle size distributions in the form of histograms are given in Fig. 2. A brief summary of previously reported microanalysis results (*12*) obtained by energy dispersive X-ray spectroscopy (EDS) is given first to facilitate discussion. The majority of particles in Ru rich sample RMH093 were below 5 nm as seen in Fig. 2a. About one-fourth of these particles gave signals for both Ru and Au whereas the remainder gave signals for Ru only. In the size range of 5 to 10 nm, the particles could be identified as either monometallic Ru or monometallic Au by EDS. Particles larger than 10 nm were, without exception, monometallic Au. The Au-rich sample, RMH014, had more large size particles than catalyst RMH093, as shown in Fig. 2b. Most of the small particles (<5 nm) gave signals for both Ru and Au. Particles between 5 and 10 nm and larger than 10 nm contained Au only. On both samples, the formation of bimetallic clusters was confined to small particle size (<5 nm). The characterization of these catalysts by a combination of different techniques is discussed in greater detail in the previous work (*12*). Microdiffraction from different metal-particle-free regions of sample RMH014 showed local variations in the MgO planes exposed. Figure 3 shows MgO patterns from different sample regions of catalyst RMH014 which were obtained without tilting the specimen. Such local variations within regions of about 1 μm are to be expected in view of the polycrystalline nature of the MgO powder used as support. Microdiffraction patterns from some specimen areas of MgO showed a splitting of diffraction spots (Fig. 3d). Splitting of diffraction spots has been previously reported for small Au particles, 2–10 nm in diameter, which were prepared by cosputtering of gold with polyester or alumina (*21*). This fine structure in the microdiffraction pattern was attributed to the phase differences associated with the relative positions of the crystal and the incident beam (*14*). The spot splitting may also result from stacking faults, twinning, and antiphase domain boundaries, especially when the incident beam is near to the edge of the particle, as illustrated by Cowley for 5-nm Pt particles (*19*). In the vicinity of Au particles, (110) planes of MgO seemed to be ex-

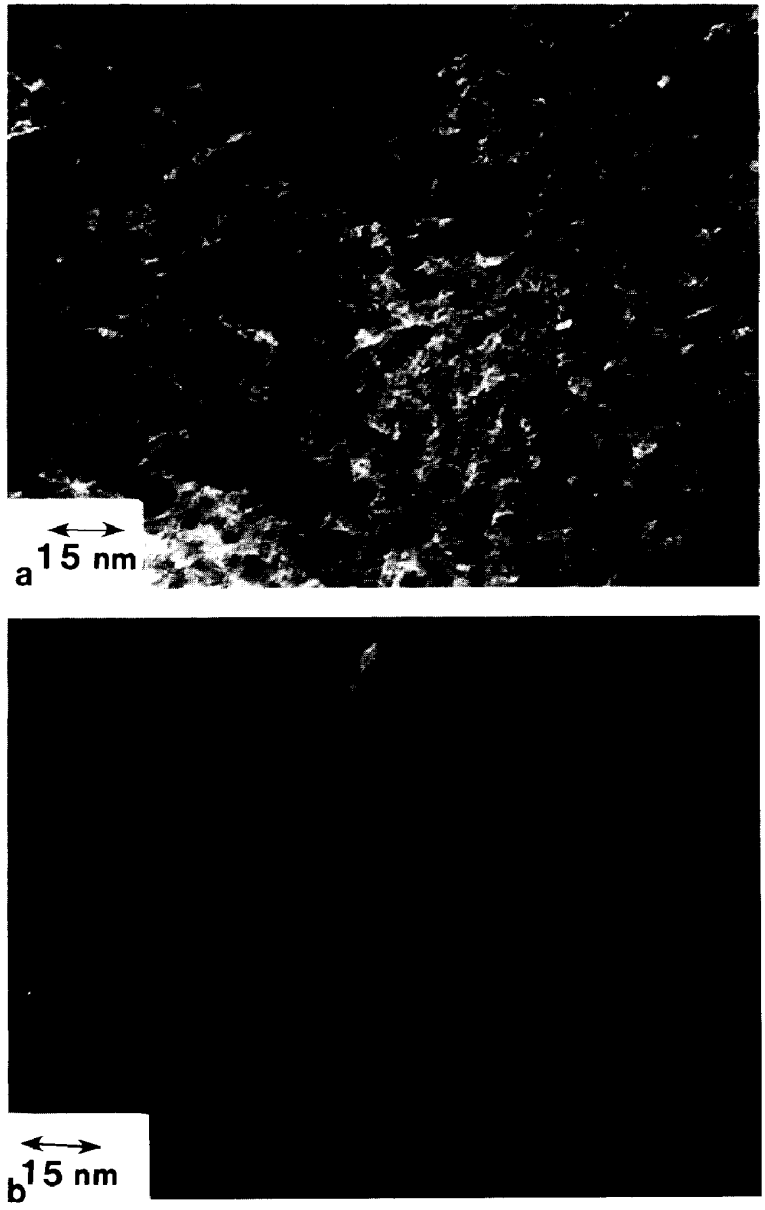

FIG. 1. Bright field transmission electron micrographs; (a) catalyst RMH093, (b) catalyst RMH014.

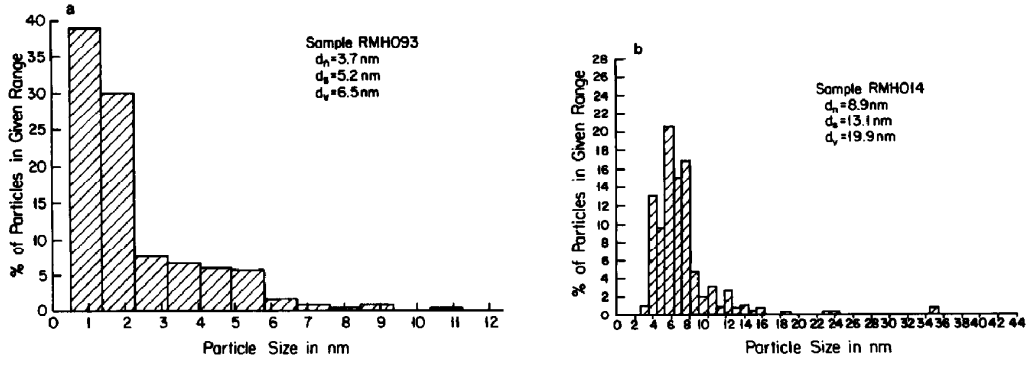

FIG. 2. Histograms showing particle size distribution; (a) catalyst RMH093, (b) catalyst RMH014.

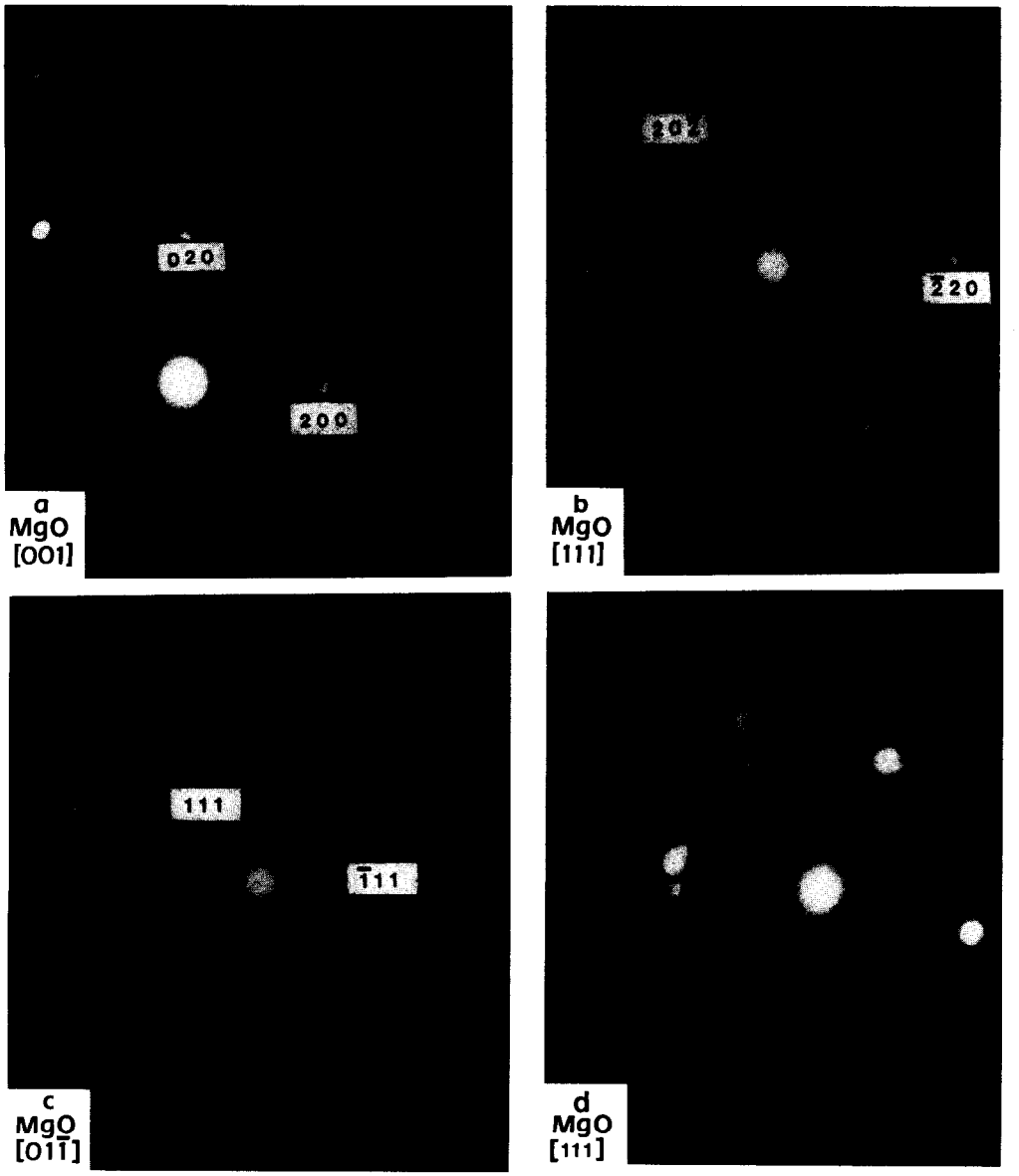

FIG. 3. Microdiffraction patterns from metal particle free regions of catalyst RMH014, showing local variations within 1 μm of specimen area; (a) MgO zone axis [001], (b) MgO zone axis [111], (c) MgO zone axis [$01\bar{1}$], (d) MgO zone axis [111] showing a splitting of diffraction spots.

posed on the surface with the electron beam parallel to the (111) plane of MgO. Figure 4 shows microdiffraction patterns of Au particles of different size obtained from catalyst RMH014. Large Au particles (>10 nm in diameter) appeared to be randomly aligned. Figures 4a and b show two patterns from such large particles corresponding to [$01\bar{1}$] and [$\bar{1}24$] zone axes, respectively. For small particles (<5 nm in diameter), the only epitaxy observed was that the [110] zone axis of Au particles was parallel to the [111] zone axis of MgO (Figs. 4c,d). An epitaxial alignment of 2-nm Au particles

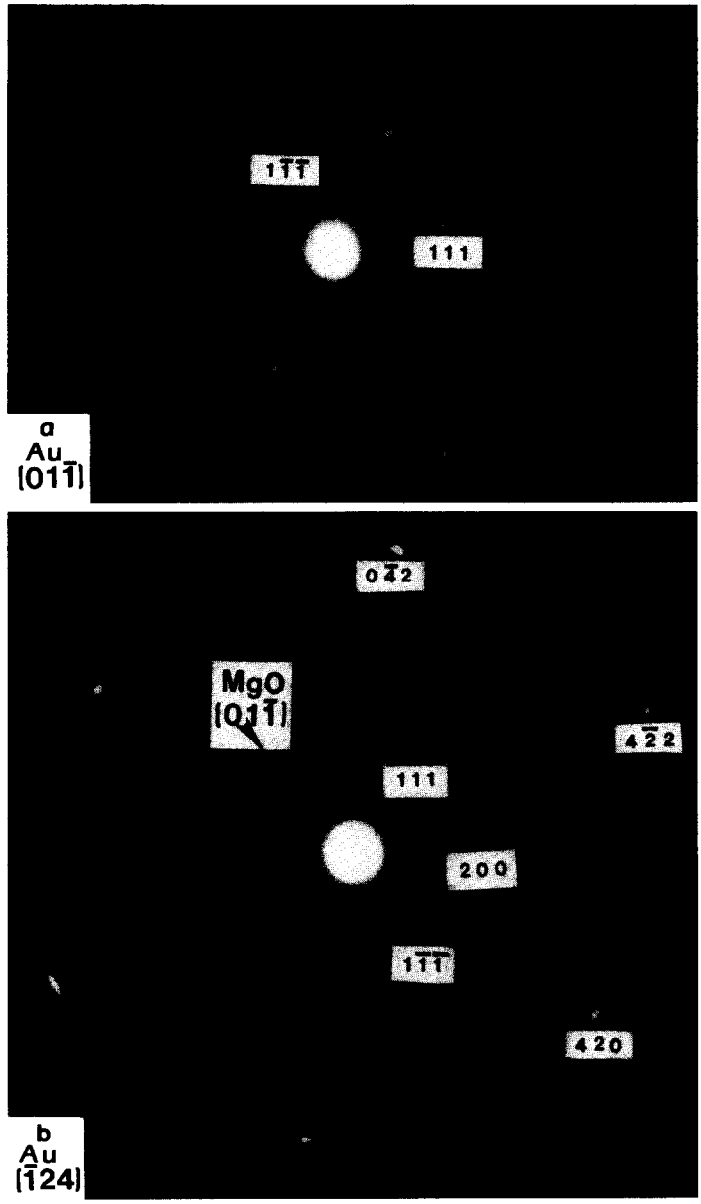

FIG. 4. Microdiffraction patterns from large Au particles (>10 nm) and small bimetallic clusters (<5 nm) of catalyst RMH014; (a) 12-nm Au particle, zone axis [01$\bar{1}$], (b) 16-nm Au particle, zone axis [$\bar{1}$24]/MgO zone axis [011], (c) 5-nm particle, multiply twinned Au/MgO zone axis [111], (d) 4-nm particle, doubly twinned Au zone axis [0$\bar{1}$1]/MgO zone axis [111].

was found on MgO smoke, prepared by an indirect exposure of oxide to the incident beam of evaporated Au atoms (*25*). In an earlier study (*26*), either epitaxial or random alignment of evaporated Au particles on MgO was found, depending on whether the oxide was vacuum-cleaved or air-cleaved. Others reported an initial growth of Au particles in [111] orientation on MgO (100) surfaces (*27*).

About 25% of the <5-nm Au particles in catalyst RMH014 showed multiple twin-

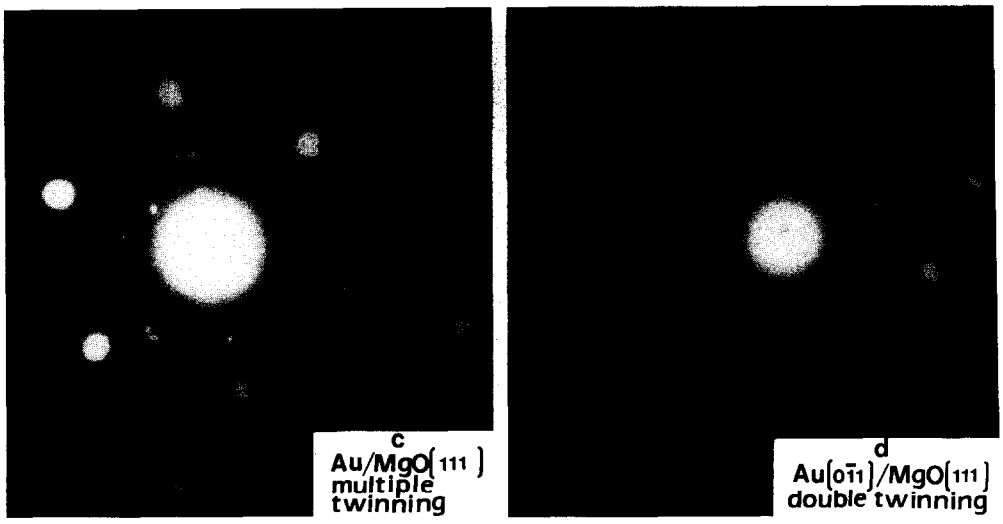

FIG. 4—*Continued.*

ning (Fig. 4c). In a previous study, a similar result was obtained, and only a small fraction (about $\frac{1}{3}$) of 1.5- to 2.0-nm Au particles showed multiple twinning (*18*) which has been proposed as the equilibrium form for very small particles of fcc metals (*22–24*). It was also seen that the probability for multiple twinning decreased as the particle size decreased for small Pt particles (*29*).

Most of the microdiffraction patterns of RMH014 could thus be ascribed to fcc Au structures. Forbidden reflections were not observed in any of the microdiffraction patterns. Forbidden reflections have been previously observed in a microdiffraction study of 10-nm Au particles on a KCl substrate and were ascribed to the presence of a large number of incomplete unit cells in the crystal (*30*). Based on EDS results (*12*) on catalyst RMH014, Ru and Au are present in a majority of the small (<5 nm) metal particles. However, the microdiffraction patterns do not indicate any structural modifications of Au, in agreement with the hypothesis that Ru–Au bimetallic clusters might consist of one metal component chemisorbed on the surface of the other (*7–12*).

On the Ru-rich sample, RMH093, most of the microdiffraction patterns could be ascribed to Ru with the [0001] zone axis of Ru parallel to the [111] zone axis of MgO. Figure 5 shows some of the microdiffraction patterns obtained. Local variations in the orientation of the MgO support were again observed (see Figs. 5a,b). The Ru particles (<5 nm in diameter) appeared to have similar alignment, irrespective of the variations in the MgO support. Some twinning of Ru was observed; however, multiple twinning was present for only a small fraction (about 20%) of the particles. No structural modification of Ru was observed in the small size range.

In both catalysts, MgO in the vicinity of metal particles was found to be highly susceptible to electron beam damage. This is in agreement with the destabilization of MgO caused by the presence of highly dispersed gold particles as reported previously (*28*).

CONCLUSIONS

An electron microdiffraction study of bimetallic Ru–Au/MgO catalysts was carried out. Local variations in the planes exposed within regions of 1 μm of the metal-particle-free MgO specimen areas were observed. Large Au particles (>10 nm) exhibited random alignment on the MgO surface. For small Au particles (<5 nm), the [110] zone

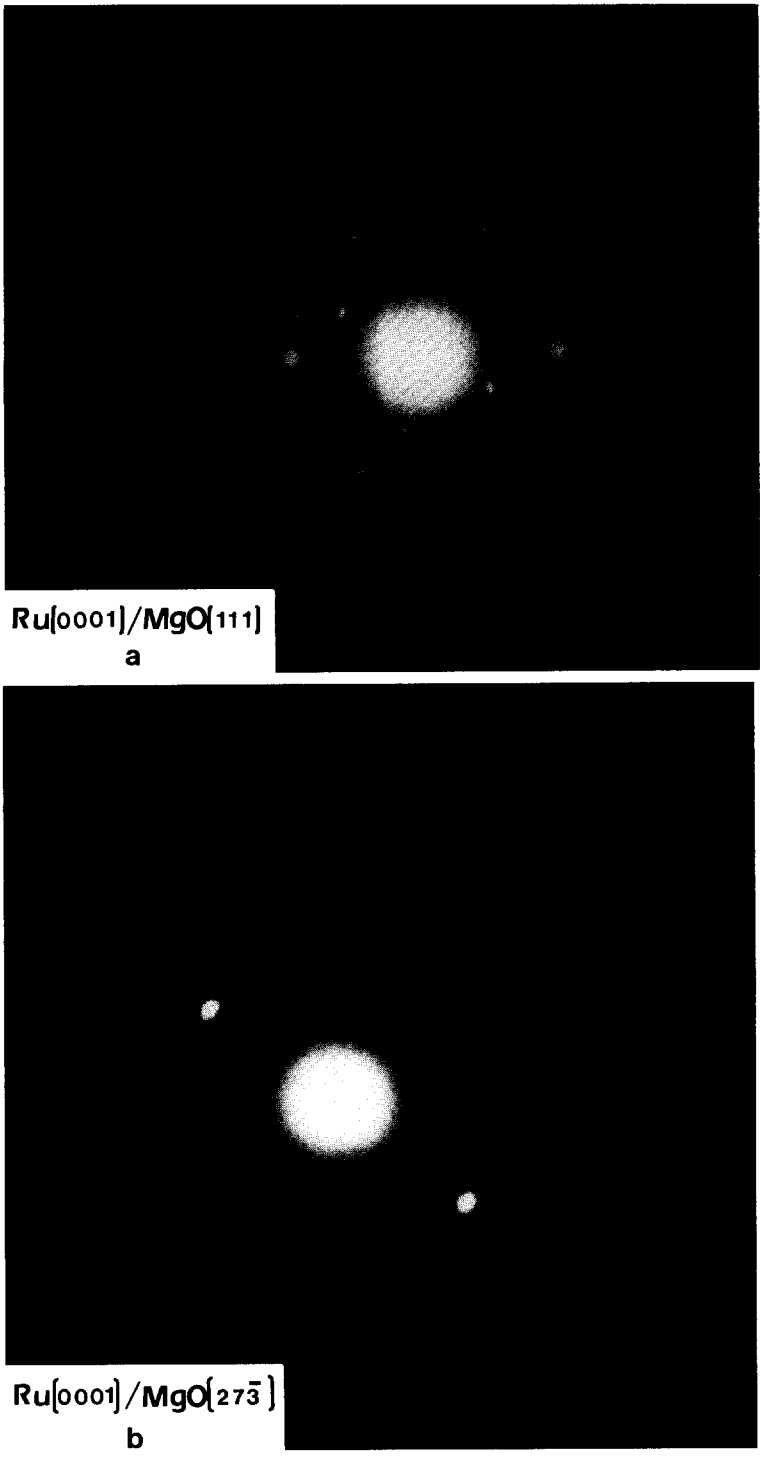

FIG. 5. Microdiffraction patterns from small particles of catalyst RMH093; (a) 4-nm particle, Ru zone axis [0001]/MgO zone axis [111], (b) 4-nm particle, Ru zone axis [0001]/MgO zone axis [27$\bar{3}$].

axis of Au was found to be parallel to the [111] zone axis of MgO. In most cases, MgO (110) planes were exposed in the vicinity of metal particles. Localized MgO regions near the metal particles showed a high susceptibility to electron beam damage. Only a small fraction of Au particles showed evidence for multiple twinning.

Ru particles (<5 nm) were aligned similarly with the (0001) planes parallel to the electron beam. In most cases the [0001] zone axis of Ru was parallel to the [111] zone axis of MgO. In small metal particles, no deviations from Ru or Au diffraction patterns were observed indicating that the "bimetallic clusters" observed by EDS can be modeled according to Sinfelt's adsorption model (*1*) where one metal component is adsorbed on the surface of the other. The "atomic ordering" model based on regular solution theory (*13*) appears to be inappropriate to describe the structure of small metal particles in bulk immiscible, bimetallic systems such as Ru–Au.

REFERENCES

1. Sinfelt, J. H., *Acc. Chem. Res.* **10,** 15 (1977).
2. Galvagno, S., and Parravano, G., *J. Catal.* **57,** 272 (1979).
3. Bassi, I. W., Garbassi, F., Vlaic, G., Marzi. A., Tauszik, G. R., Cocco, G., Galvagno, S., and Parravano, G., *J. Catal.* **64,** 405 (1980).
4. Galvagno, S., Schwank, J., Parravano, G., Garbassi, F., Marzi, A., and Tauszik, G. R., *J. Catal.* **69,** 283 (1981).
5. Tauszik, G. R., Leofanti, G., and Galvagno, S., *J. Mol. Catal.* **25,** 357 (1984).
6. Galvagno, S., Schwank, J., and Parravano, G., *J. Catal.* **61,** 223 (1980).
7. Datye, A. K., and Schwank, J., *in* "Proceedings, 8th International Congress on Catalysis, Berlin," Vol. IV, p. 587. Verlag Chemie, Weinheim, 1984.
8. Datye, A. K., and Schwank, J., *J. Catal.* **93,** 256 (1985).
9. Datye, A. K., Lee, J. Y., Shastri, A. G., and Schwank, J., AIChE Annual Meeting, 1984, San Francisco, Calif., Paper No. 53a.
10. Shastri, A. G., and Schwank, J., *J. Catal.* **95,** 271 (1985).
11. Shastri, A. G., and Schwank, J., *J. Catal.* **95,** 284 (1985).
12. Shastri, A. G., and Schwank, J., *J. Catal.* **98,** 191 (1986).
13. Balseiro, C. A., and Moran-Lopez, J. L., *Surf. Sci.* **156,** 404 (1985).
14. Cowley, J. M., and Spence, J. C. H., *Ultramicroscopy* **6,** 359 (1981).
15. Cowley, J. M., *Ultramicroscopy* **8,** 1 (1982).
16. Turner, P. S., and Cowley, J. M., *Ultramicroscopy* **6,** 135 (1981).
17. Cowley, J. M., and Monosmith, W. B., *in* "Proceedings, 41st Annual Meeting of the Electron Microscopy Society of America" (G. W. Baily, Ed.), p. 332. San Francisco Press, San Francisco, 1983.
18. Monosmith, W. B., and Cowley, J. M., *Ultramicroscopy* **12,** 177 (1984).
19. Cowley, J. M., *J. Microsc.* **129,** 253 (1983).
20. Cowley, J. M., ACS Symposia Series on "The New Surface Science in Catalysis," Vol. 29, No. 3, Aug. 1984, Philadelphia, Pa.
21. Roy, R. A., Messier, R., and Cowley, J. M., *Thin Solid Films* **79,** 207 (1979).
22. Allpress, J. A., and Sanders, J. Y., *Surf. Sci.* **7,** 1 (1965).
23. Fukano, Y., and Wayman, C. M., *J. Appl. Phys.* **40,** 1656 (1969).
24. Ino, S., *J. Phys. Soc. Japan* **27,** 941 (1969).
25. Cowley, J. M., and Neuman, K. D., *Surf. Sci.* **145,** 301 (1984).
26. Green, A. K., Dancy, J., and Bauer, E., *J. Vacuum. Sci. Technol.* **7,** 159 (1970).
27. Takayanagi, K., Yagi, K., and Honjo, G., *Thin Solid Films* **48,** 137 (1978).
28. Schwank, J., Shastri, A. G., and Lee, J. Y., ACS Symposium Series on "Strong Metal Support Interactions" (R. T. Baker, S. J. Tauster, and J. A. Dumesic, Eds.), Vol. 298, p. 182. Amer. Chem. Soc., Washington, D.C., 1986.
29. Cowley, J. M., and Kang, Z. C., *Ultramicroscopy* **11,** 131 (1983).
30. Castano, V., Gomez, A., and Jose-Yacaman, M., *in* "Proceedings, 42nd Annual Meeting of the Electron Microscopy Society of America" (G. W. Baily, Ed.), p. 658. San Francisco Press, San Francisco, 1984.
31. Cowley, J. M., "Diffraction Physics." North-Holland, Amsterdam, 1975.
32. Lynch, J. P., Lesage, E., Dexpert, H., and Freund, E., *in* "Inst. Phys. Conf. Ser. No. 61," Chap. 2, p. 67. Cambridge, Sept. 1981.
33. Klier, K., Simmons, G. W., Himelfarb, P. B., and Jose-Yacaman, M., ACS Symposium on "The New Surface Science in Catalysis," p. 281. Aug. 1984, Philadelphia Pa.